International Journal of Fracture **114:** 87–111, 2002.

Evaluation of crack tip fields and stress intensity factors in functionally graded elastic materials: Cracks parallel to elastic gradient

C.-E. ROUSSEAU and H.V. TIPPUR*

*Department of Mechanical Engineering, Auburn University, Auburn, AL 36849, U.S.A. (*Author for correspondence, e-mail: htippur@eng.auburn.edu)*

Received 1 February 2000; accepted in revised form 7 January 2002

Abstract. Particulate functionally graded materials (FGM) made of glass-filled epoxy with edge cracks parallel to the direction of the elastic gradient and subjected to pure bending have been studied. Crack tip measurements are used to examine continuum models for FGMs by treating the material as isotropic and nonhomogeneous at macroscales. Situations where cracks are located on the compliant and the stiff sides of the beams are separately examined by mapping crack tip deformations using optical interferometry. Comparative experiments on homogeneous compositions corresponding to identical elastic properties of the crack tip region in the FGM are also undertaken. A methodology for extracting fracture parameters in FGMs based on locally homogeneous material descriptions is advanced. Companion finite element models are used to aid the development of fringe analysis procedures and to provide a direct comparison to the optical measurements. Stress intensity factors in FGMs are compared to each other and to their homogeneous counterparts. Optical measurements near quasi-statically growing cracks in FGMs have been undertaken, and crack growth resistance behavior is explained using crack initiation toughness variation as a function of filler volume fraction in homogeneous sheets.

Key words: Crack tip fields, finite element analysis, functionally graded material, glass-filled epoxy composite, nonhomogeneity, optical interferometry, stress intensity factors.

1. Introduction

Functionally Graded Materials (FGMs) have spatially varying composition and mechanical properties. The gradual variation in material composition instead of sharp interfaces as in the case of multilayered systems significantly improves the thermal and mechanical characteristics of FGMs. Therefore, they are currently considered for many demanding engineering applications including military armor, earth moving equipment, thermal barrier coatings for turbine blades and internal combustion engines, machine tools and so on. In view of the attractive mechanical and thermal characteristics, several investigators have explored fracture behavior of FGMs. Of interest. here is the condition in which a crack parallel to the elastic modulus gradient is present in the FGM. One of the early works pertaining to a crack parallel to the elastic modulus of an FGM was undertaken by Delale and Erdogan (1983) who suggested the stress singularity at the crack tip to have the standard $1/\sqrt{r}$ from which was confirmed by Eischen (1987). Jin and Noda (1994) concluded likewise, independently of the crack orientation relative to the property gradient. Applying the crack-bridging concept, Jin and Batra (1996) have shown that fracture toughness in alumina-nickel FGMs increases as the crack propagates from the ceramic-rich into the metal-rich region. In a paper summarizing

recent advances in fracture of FGMs, Erdogan (1995) has presented theoretical results for cracks along the gradient direction, under various loading conditions.

The works mentioned above are of a theoretical and/or numerical nature. To date, very few experimental mechanics investigations on FGM fracture mechanics are reported. At present, compositionally graded mixtures seem to hold a great deal of promise for commercial production and experimental examination. Butcher et al. (1999) have proposed a compositionally graded glass-filled epoxy for experimental mechanics investigations. Direct evaluation of crack tip deformations and Stress Intensity Factors (SIF) in two-phase particulate FGMs with continuous Young's modulus variation was reported by them. They studied an FGM with a crack perpendicular to the direction of the gradient using optical measurements and observed enhancement of crack initiation toughness in graded systems when compared to bimaterials. Marur and Tippur (1998) developed an elastic impact method for characterizing the elastic properties of such particulate composites. More recently, a particulate FGM made of cenospheres in polyester matrix has been developed and elastic and mechanical strength characteristics are evaluated by Parameswaran and Shukla (2000).

The present investigation is aimed towards direct measurement of crack tip deformation and fracture parameters in compositionally graded particulate FGMs. The influence of elastic gradients on crack tip deformations and the fracture parameters are examined when the cracks are oriented parallel to the elastic gradient. The possibility of using singular and/or asymptotic expansions available for homogeneous materials to extract stress intensity factors from measured optical interferograms is addressed and the issue of K-dominance is examined. The experimental investigation is complemented with the aid of companion finite element modeling of the experiments to provide a direct comparison. Measurements are utilized to provide an assessment of fracture performance of FGMs relative to homogeneous counterparts. Quasi-static crack growth in these FGMs is investigated and the behavior is reconciled with experimentally measured crack initiation toughness of homogeneous counterparts of different but constant volume fraction.

In the next section theoretical background on FGMs is briefly presented. Finite element analysis of the crack tip fields to aid fringe analysis and extraction of fracture parameters is included in Section 3. Guidelines are set which help to establish a formulation for the stress distribution pattern in the vicinity of an FGM crack. It serves as an essential foundation of the experimental evaluation. This section also includes a novel method for imposing elastic modulus variation in the FGM. Section 4 provides pertinent details of the FGM sample preparation, material characterization, and the optical measurements of crack tip deformation. Finally, in Section 5, the experimental results obtained using the methods developed are compared with those computed numerically. A method of evaluation stress intensity factors for FGMs is posed and resistance of this material to crack extension is investigated.

2. Theoretical background

Consider a planar isotropic nonhomogeneous medium with a smooth unidirectional variation in Young's modulus in the x-direction and a constant Poisson's ratio. Let a crack be oriented along the x-axis with crack tip at the origin as shown in Figure 1. For the problem of symmetric loading, the dominant crack tip stress field is shown to be (Eischen, 1987),

$$\sigma_{ij}(r,\theta) \cong \frac{K_I}{\sqrt{2\pi r}} f_{ij}^I(\theta) + O(r^{1/2}), \quad (i,j = x,y), \tag{1}$$

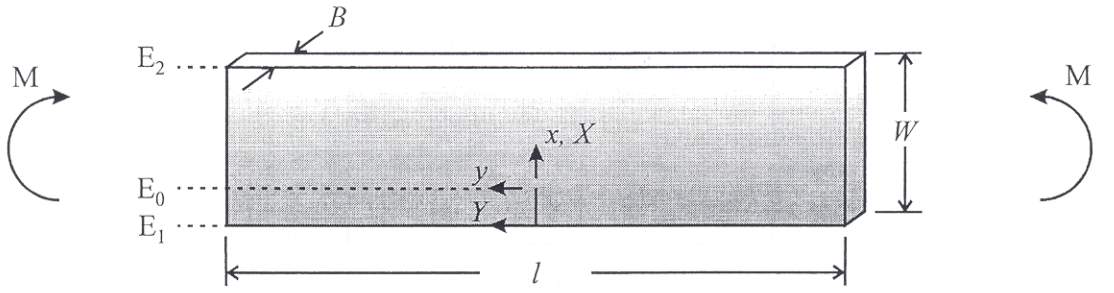

Figure 1. Schematic of a Functionally Graded strip.

where K_I is the mode I stress intensity factor, and r and θ are the crack tip polar coordinates. The functions f_{ij}^I are identical to the universal angular functions for homogeneous materials. Thus, in the near tip region, the stress singularity in FGMs is identical to that of homogeneous materials, and is unaffected by the material property gradient. In the same work, it has also been demonstrated that the first terms of the asymptotic displacement fields of FGMs, proportional to $r^{1/2}$, r^0, and r^1, are identical to those of homogeneous materials, thus are independent of the gradient. Erdogan (1995) has developed near tip expressions for stress fields in nonhomogeneous planar bodies that include the influence of elastic property gradients. For an exponential variation of elastic modulus of the form,

$$E(x) = E_0 e^{\alpha x} = E_0 e^{r\alpha \cos\theta}, \tag{2}$$

where E_0 is the Young's modulus at the origin, and α is a scalar dependent on the terminal values of the modulus and the length of the graded region, the near tip stresses are shown to be of the form,

$$\sigma_{ij}(r,\theta) \cong e^{r\alpha \cos\theta} \left(\frac{K_I}{\sqrt{2\pi r}} f_{ij}^I(\theta) \right), \quad (i, j = x, y). \tag{3}$$

In the limit as $r \to 0$, Equation (3) reduces to Equation (1).

3. Finite element simulations

Numerical simulations of cracked FGM samples, using the ANSYS^{TM} finite element package, were first carried out to understand the features of the measured crack tip field and formulate a basis for extracting stress intensity factors from the measured deformations. *Plane stress elasto-static simulations* of cracked beams subjected to pure bending were performed for both FGMs and homogeneous materials. In the case of FGM beams, the measured Young's modulus gradient from the samples used in the experiments, to be discussed in the next section, was prescribed. However, the Poisson's ratio was kept constant at a value corresponding to that of the crack tip, throughout the finite element model. Separate simulations were carried out for situations with the crack located on the stiff and the compliant sides of FGM beams. The corresponding crack tip elastic properties were used in separate homogeneous beam simulations. Due to symmetry, only half of the specimens were represented in the numerical simulations. A typical model consisted of 7100 eight-noded isoparametric elements with 22 000 nodes and two degrees of freedom per node, as shown in Figure 2. The mesh was created with a strong bias towards concentrating a large number of elements in the crack tip vicinity. The smallest

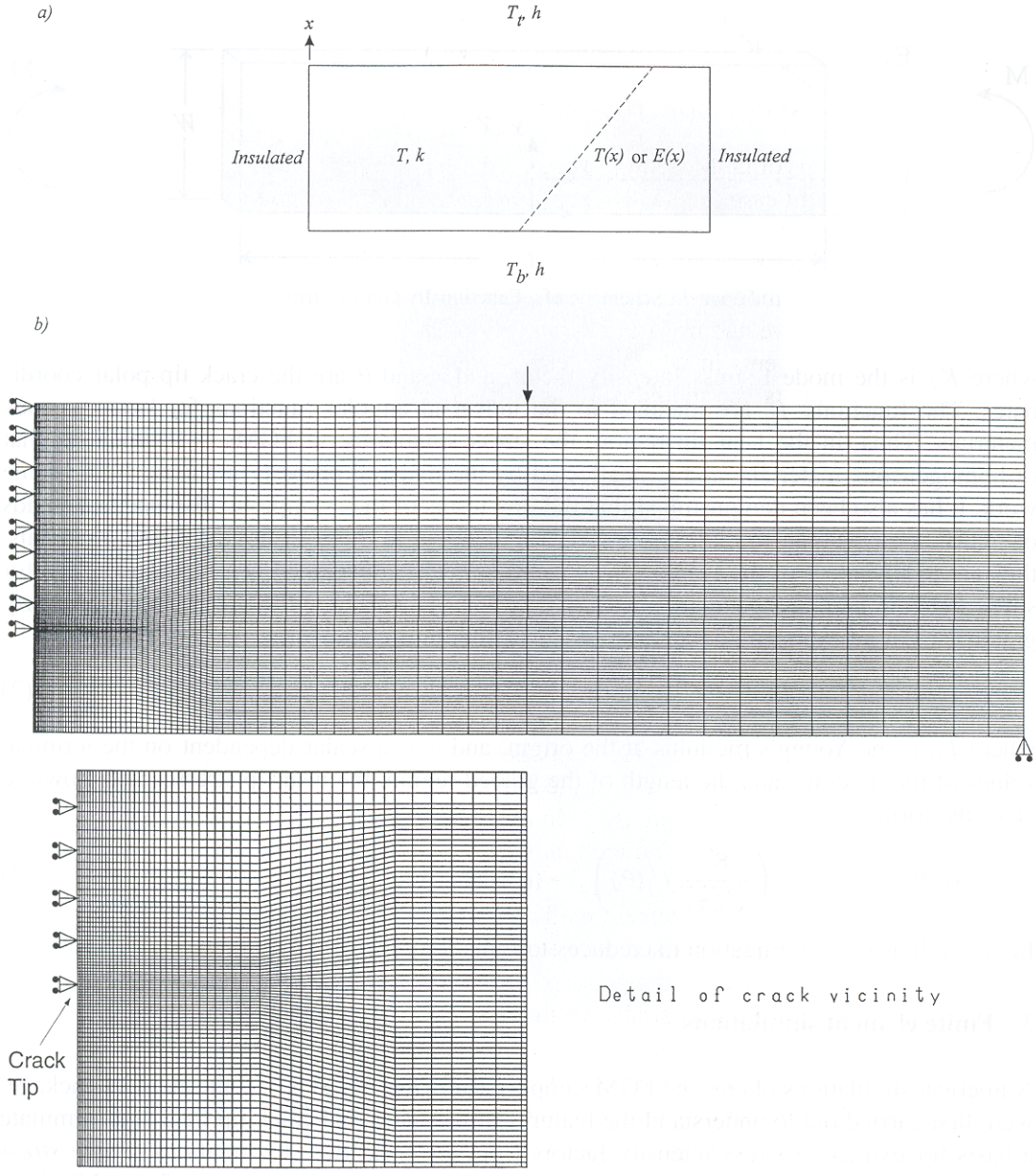

Figure 2. Numerical model: (a) thermomechanical analysis to apply Young's modulus variation, (b) finite element discretization.

elements near the crack tip measured 100 μm in size. In the vertical direction, 90 elements were used, while 79 elements existed, in the horizontal direction. No special crack tip elements (such as singular elements) were used in the model.

It should also be noted that the adequacy of the degree of discretization of the finite element model was determined by generating a coarse mesh and progressively reducing element size. Element sizes were progressively reduced by a factor of 60%. The process was automated by writing a model generation macro within the ANSYS^{TM} software package. Convergence was

deemed satisfactory once the difference between the values of stress intensity factor computed (to be discussed in Section 3.2) from two consecutive models was less than 1%.

3.1. Implementation of Young's modulus gradient in FGM model

Numerical simulations of FGMs require implementing the required property variation, Young's modulus in the present case, in the discretized domain. This is generally done by discretizing a rectangular domain into rows (or columns) of elements and imposing a constant value of Young's modulus to each row of elements (Butcher et al., 1999; Bao and Cai, 1997). Thus, a stepwise change in modulus can be realized. Alternatively, a piecewise linear variation would be more attractive and precise. Lee and Erdogan (1995) have formulated higher order nonhomogeneous elements in which the elastic matrix is a function of spatial coordinates, thus integrally accounts for modulus variations. Giannakopoulos and Suresh (1997) have developed a subroutine to be used with ABAQUS^{TM} to implement varying distributions in material properties within individual elements. In the present work, a new method involving standard modules available in most finite element software packages is utilized to implement a linear variation of Young's modulus within an element. A brief description of the method is as follows.

Consider a rectangular homogeneous isotropic continuum with an arbitrary uniform thermal conductivity k and a uniform initial temperature T (Figure 2). Let the vertical edges be insulated as shown. Assume further that the convective heat transfer coefficients for the top and bottom surfaces have the same arbitrary value, h. When this body is subjected to temperatures T_b and T_t at the bottom and top edges, respectively, upon reaching steady state, a linear temperature gradient varying from T_t at the top edge to T_b at the bottom edge is realized. Discretizing the domain into finite elements and solving the governing equation for steady state heat flow will therefore result in linearly varying nodal temperatures with respect to position in the vertical (or, x-) direction. (If needed, non-linear temperature distributions could be implemented in several ways, for instance, by introducing heat generation rates at strategic locations of the finite element model.)

The nodal temperatures obtained above can be used as thermal loading into a structural finite element model. However, temperature variations will induce thermal mismatch, hence thermal stresses which are undesirable in the present work. This can be remedied easily by setting the coefficient of thermal expansion α_0 to zero, thus returning the material to its stress free condition. Finally, defining material properties (in this case Young's modulus for the FGM) as linear functions of temperature result in the desired nodal material property variation which follows the temperature gradient precisely.

3.2. Path-independent integral and numerical evaluation of K_I

The path-independent integral developed by Rice (1968) is valid for homogeneous materials, bimaterials, and FGMs with elastic gradient perpendicular to direction of the crack. However, path independence is lost when the elastic gradient is parallel to the direction of the crack in non-homogeneous materials. Eischen (1987) has introduced a path independent integral J^* which incorporates an additional integral to Rice's line integral to restore path independence. Based on the assumptions of isotropy, linear elasticity, and smoothly varying elastic modulus, Honein and Herrmann (1997) have developed a path independent integral, J_e, for nonhomogeneous materials. Although plane strain conditions have been used in the derivations, the validity of the results for both plane stress and three-dimensional problems is asserted in

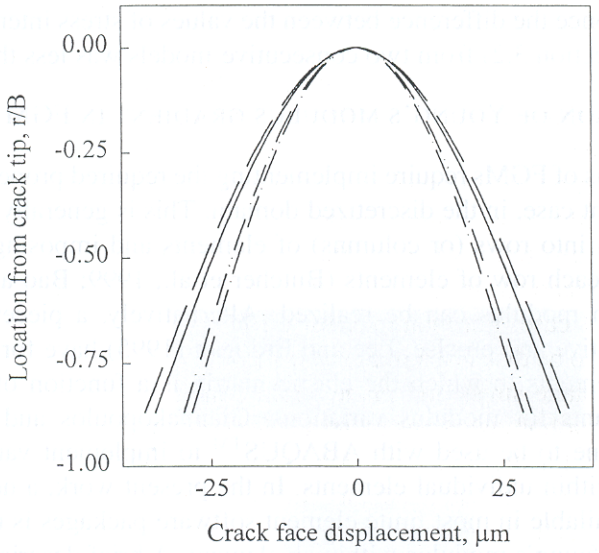

Figure 3. Crack opening displacement in FGM ($E_2/E_1 = 0.4$) for plane stress (solid line) and plane strain (long dash) conditions and for homogeneous material ($E_0 = 6.8$ GPa) for plane stress (dash-dot) and plane strain (short-dash) conditions.

Honein and Hermann (1997). For an exponential form of the modulus variation, J_e is given by,

$$J_e = \oint_{\partial\Omega} \left[W\delta_{1i} - \sigma_{ij}\frac{\partial u_j}{\partial x_1} - \frac{\alpha}{2}u_j\sigma_{ij} \right] n_i \, \mathrm{d}l \quad i, j = x, y, \tag{4}$$

where W is the strain energy density, $\partial\Omega$ is the boundary of the domain of the integral, and n_i is the outward normal to the inner boundary of the domain. It is seen that setting the elastic gradient parameter $\alpha = 0$, reduces Equation (4) to the standard J-integral for homogeneous materials. Further, for plane stress and mode-I conditions, J_e is related to the stress intensity factor as,

$$J_e = \frac{1}{E_0}(K_I^2). \tag{5}$$

Note the use of crack tip values of elastic modulus in Equation (5). In this study, Equations (4) and (5) were used in determining the mode-I stress intensity factors from the plane stress numerical simulations of cracked FGM beams.

This methodology was further verified by comparison with stress intensity factor evaluation from crack opening displacement. The latter has been bench-marked and used by Marur and Tippur (2000) and Rousseau and Tippur (2000) to determine dynamic and static stress intensity factors, respectively, in FGMs with cracks normal to the elastic gradient direction. It was also adopted successfully by Rousseau and Tippur (2001) in evaluating the dynamic behavior of FGMs having cracks parallel to the elastic gradient. The two methods resulted in stress intensity factor differences of less than 2% (Rousseau, 2000).

3.3. Validity of planar assumptions

It is well known that conditions near an elastic crack tip generally are neither plane stress nor plane strain, but rather three-dimensional (Rosakis and Ravi-Chandar, 1987) in finite thickness samples. In homogeneous materials, plane strain conditions are anticipated on the mid-plane of the sample while regions on the surface, at distances r greater than one-half plate thickness from the crack tip, could be well approximated by plane stress behavior. Between these two extremes exists the three-dimensional situation. In view of the finite thickness FGM samples studied in this work, plane stress and plane strain models were studied as extreme situations of a three-dimensional case. For example, for an FGM with $E_2/E_1 = 0.41$ (geometry and loading configuration to be discussed in the next sub-section) two finite element analyses were conducted assuming plane stress and plane strain conditions, respectively. Similar analyses were also carried out for homogeneous materials for comparative purposes. In Figure 3, crack opening displacements for the FGM and homogeneous cases, subjected to identical loading, are presented. Crack opening displacements for plane stress case are more than for the ones for plane strain case in bath FGM and homogeneous materials. It is also evident that the plane stress/plane strain difference in crack face opening is similar between FGMs and homogeneous materials. In addition, similar stress variations for plane stress and plane strain between the two materials are observed. As an example, variation of crack opening stress ahead of the crack along $(x, y = 0)$ is shown in Figure 4. The difference in plane stress/plane strain stresses between the two material is relatively constant, in each case around 15%. Due to these similarities in plane stress/plane strain displacements and stresses for homogeneous and FGM cases, it is reasonable to anticipate three-dimensionality near the FGM crack tip to be similar to the one in the homogeneous material as well.

3.4. Computed deformation fields in FGMs

Numerical simulations were performed to guide companion experimental work. The specimen geometry and the material properties used in the computational work complement the ones used in the experimentation. Results from these finite element simulations and their implication to experimental analysis are discussed next.

Far-field stresses and deformations.

The variation of far-field stress σ_y (at a location $y = W$) in the direction of Young's modulus gradient is plotted for both homogeneous and FGM beams of dimensions 120 mm $\times$ 20 mm $\times$ 6 mm in Figure 5a. These results correspond to the case of a crack situated on the stiff side of the FGM. (Note that in the far-field $(\sigma_x + \sigma_y) \approx \sigma_y$ as $\sigma_x << \sigma_y$.) In the case of the FGM beam, the stress variation is nonlinear. The stress variation for the homogeneous beam is linear as expected.

Experimental measurements are generally displacements and/or density changes. In the current investigation the optical measurements are related to out-of-plane displacements $w \propto ((\sigma_x + \sigma_y)/E(x))$, see Section 4.2. Accordingly, this quantity is plotted in Figure 5b and shows different but linear variation for both FGM and homogeneous beams. The experimental method used here Coherent Gradient Sensing, CGS, being a measure of the gradient of w in the x-direction, the far-field response is thus one of uniform fringe. Hence, it can be concluded that the functional form (linear in this case) of the far-field behavior of the measured quantity

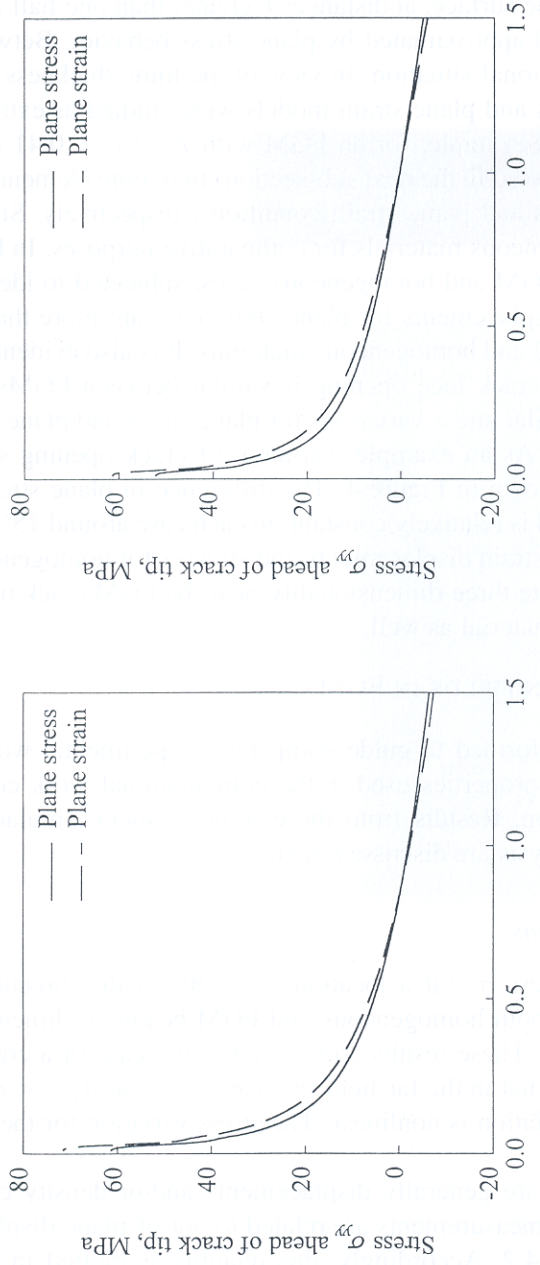

Figure 4. Stress variation ahead of crack tip in (a) FGM ($E_2/E_1 = 0.4$) and (b) homogeneous material ($E_2 = 6.8$ GPa) for plane stress and plane strain conditions

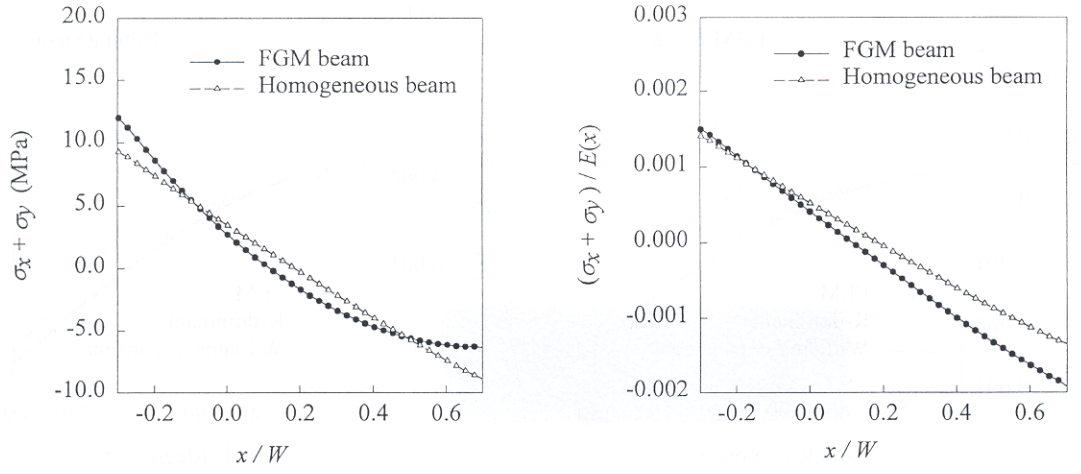

Figure 5. Stress variation in far-field: (a) in-plane stresses, (b) normalized by $E(x)$, in FGMs with edge crack on stiff side, and their homogeneous counterparts. Applied far field stress $(6M/BW^2) \sim 10.2$ MPa.

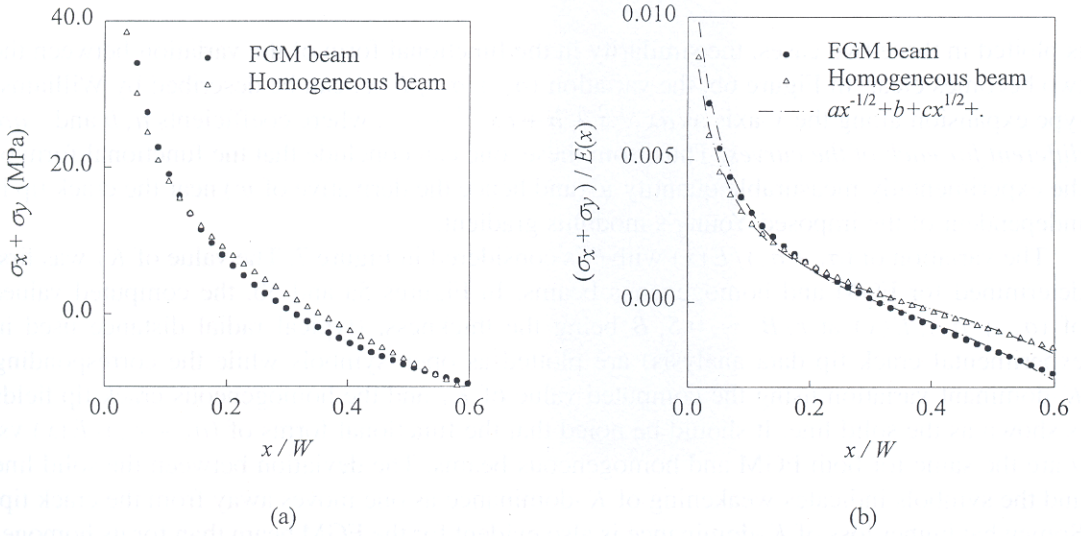

Figure 6. Stress variation ahead of the crack: (a) in-plane stresses, (b) normalized by $E(x)$, in FGMs with edge crack on stiff side, and their homogeneous counterparts. Applied far field stress $(6M/BW^2) \sim 10.2$ MPa.

from CGS in FGM and homogeneous samples are the same. This point is reinforced and illustrated by CGS fringe patterns in Section 4.3.

Near tip stresses and deformations.

The variation of stress $(\sigma_x + \sigma_y)$ along the x-axis near the crack tip is plotted in Figure 6a for the FGM with a crack on the stiffer side, along with its homogeneous counterpart. Both variations show an asymptotic behavior very close to the crack tip $(r \to 0)$ as expected from Equation (1). However, the variation is linear far from the crack tip in the homogeneous beam while remaining nonlinear for the FGM beam. Again when the quantity $(\sigma_x + \sigma_y)/E(x) (\propto w)$

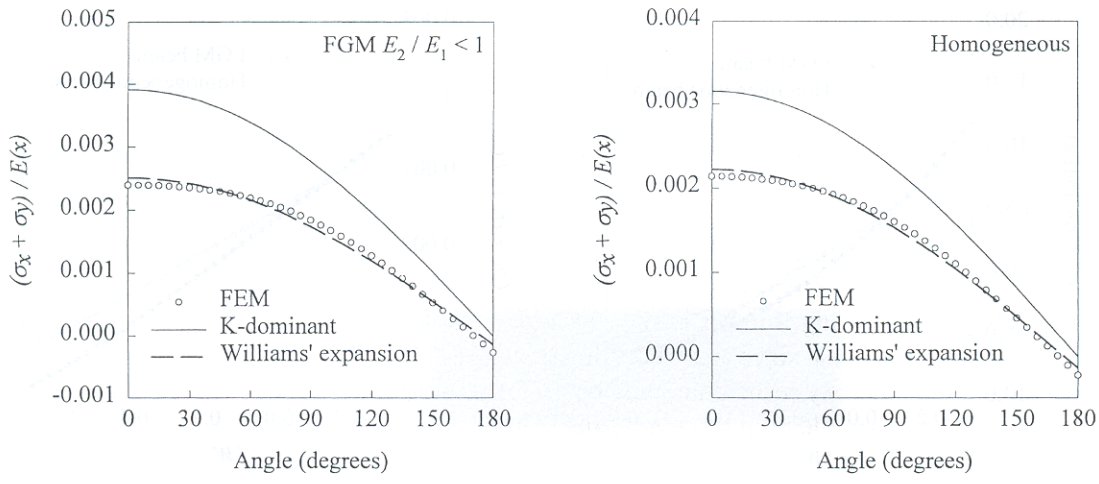

Figure 7. Normalized stress distribution at $r/a \sim 0.5$ for (a) FGM with crack on stiff side, and (b) its homogeneous counterpart. Applied far field stress $(6M/BW^2) \sim 10.2$ MPa.

is plotted in these two cases, the similarity in the functional form of the variation between the two becomes clear. In Figure 6b, the variation $(\sigma_x + \sigma_y)/E(x)$ can be described by Williams' type expansion along the x-axis as $ax^{-1/2} + b + cx^{1/2} + \cdots$, where coefficients a, b and c *are different for each of the curves*. Thus from these, one can conclude that the functional form of the experimentally measurable quantity w (and hence the derivative of w) near the crack tip is independent of the imposed Young's modulus gradient.

The variation of $(\sigma_x + \sigma_y)/E(x)$ with θ is considered in Figure 7. The value of K_I was first determined for FGM and homogeneous beams. In Figures 5a and 5b, the computed values of $(\sigma_x + \sigma_y)/E(x)$ at $r/B \sim 0.5$, B being the thickness, (typical radial distance used in experimental crack tip data analysis) are plotted as open symbols while the corresponding K-dominant variation using the computed value of K_I and the homogeneous crack tip fields is shown as the solid line. It should be noted that the functional forms of $(\sigma_x + \sigma_y)/E(x)$ vs. θ are the same for both FGM and homogeneous beams. The deviation between the solid line and the symbols indicates weakening of K-dominance as one moves away from the crack tip. Somewhat higher loss of K-dominance is also evident for the FGM beam than for its homogeneous counterpart. The method for dealing with diminishing K-dominance in homogeneous materials is to incorporate non-singular terms using Williams' expansion field (Williams, 1957) in addition to the K-dominant term. Accordingly, when two non-singular terms from Williams' expansion field (coefficients of r^0 and $r^{1/2}$) were used with the K-dominant term, good agreement between the computed field and the asymptotic field was obtained. The result is shown as the broken line in Figure 7b. Since the functional form of $(\sigma_x + \sigma_y)/E(x)$ for the FGM and homogeneous beams are the same, use of Williams' expansion field is also attempted for the FGM. In Figure 7a, the broken line corresponds to the use of two additional terms from the Williams' expansion field along with the K-dominant term to describe the computed field. As in the homogeneous counterpart, the agreement between the broken line and the open symbols is excellent. Hence, Williams' expansion field could also be used for analyzing the out-of-plane displacement data.

4. Experimental work

4.1. Material and its elastic properties

All FGM samples used for this work consisted of an epoxy matrix (Young's modulus $\sim$ 3 GPa, Poisson's ratio ~ 0.35) in which varying quantities of solid A-glass spheres (mean diameter $\sim 42\ \mu$m, Young's modulus $\sim$ 69 GPa, Poisson's ratio ~ 0.15) provided the variation in elastic properties. Gravity casting was used to reach the desired gradation. Ultrasonic pulse-echo and beam deflection measurements were used to determine the variations in Young's modulus and Poisson's ratio, following Butcher et al. (1999).

It should be noted that since we are dealing with a heterogeneous mixture of solid spherical glass inclusions in epoxy resin, care must be exercised to ensure that the inclusions are much smaller than the 'sample' dimensions (Huet, 1990; Ostoja-Starzewski, 1996) for property homogenization to be valid. That is, the representative volume element concept holds for the applying micro-mechanics models and characterize material properties over the element dimensions is preserved. As described in Butcher et al. (1999), the transducer (ultrasonic or strain-gage) dimensions as well as the sample dimensions used in this work were of the order of a millimeter and were generally two orders of magnitude larger than the mean inclusion size of $\sim 42\ \mu$m. Even the initial notch thickness cut into the samples, were over seven times the size of the inclusions.

Figures 8a and 8b show the measured Young's modulus (open symbols) and Poisson's ratio variation of *homogeneous mixtures* having different but constant volume fractions of glass filler in the epoxy matrix. A Young's modulus variation from about 3 to 9 GPa and a Poisson's ratio variation from 0.35 to 0.29 is seen when the volume fraction of the filler is increased from zero to 0.5. (It should be noted that these particulate composites show a nominally linear load-displacement behavior (Butcher et al., 1999)). Also included in Figure 8a are micromechanics based predictions of the elastic modulus variation of the particulate composite based on (a) Mori-Tanaka method (Weng, 1984) and (b) Halpin-Tsai ('rule-of-mixtures') prediction (SEM Monograph, 1984) for different volume fractions V_f. In the former method, the bulk modulus κ and the shear modulus μ of the composite are expressed in terms of the corresponding values of the matrix and the filler material as,

$$\kappa = \kappa_m \left[1 + \frac{V_f}{\dfrac{3\left(1 - V_f\right)\kappa_m}{3\kappa_m + 4\mu_m} + \dfrac{\kappa_m}{\kappa_i - \kappa_m}} \right], \tag{6}$$

$$\mu = \mu_m \left[1 + \frac{V_f}{\dfrac{6}{5}\dfrac{\left(1 - V_f\right)\left(\kappa_m + 2\mu_m\right)}{3\kappa_m + 4\mu_m} + \dfrac{\mu_m}{\mu_i - \mu_m}} \right], \tag{7}$$

where subscripts m and i denote the matrix and the inclusions, respectively. The Young's modulus and Poisson's ratio of the composite is obtained from the above two moduli by knowing $\kappa = E/3(1 - 2v)$, and $\mu = E/2(1 + v)$. The Halpin–Tsai estimate for the elastic modulus of the composite material is given by,

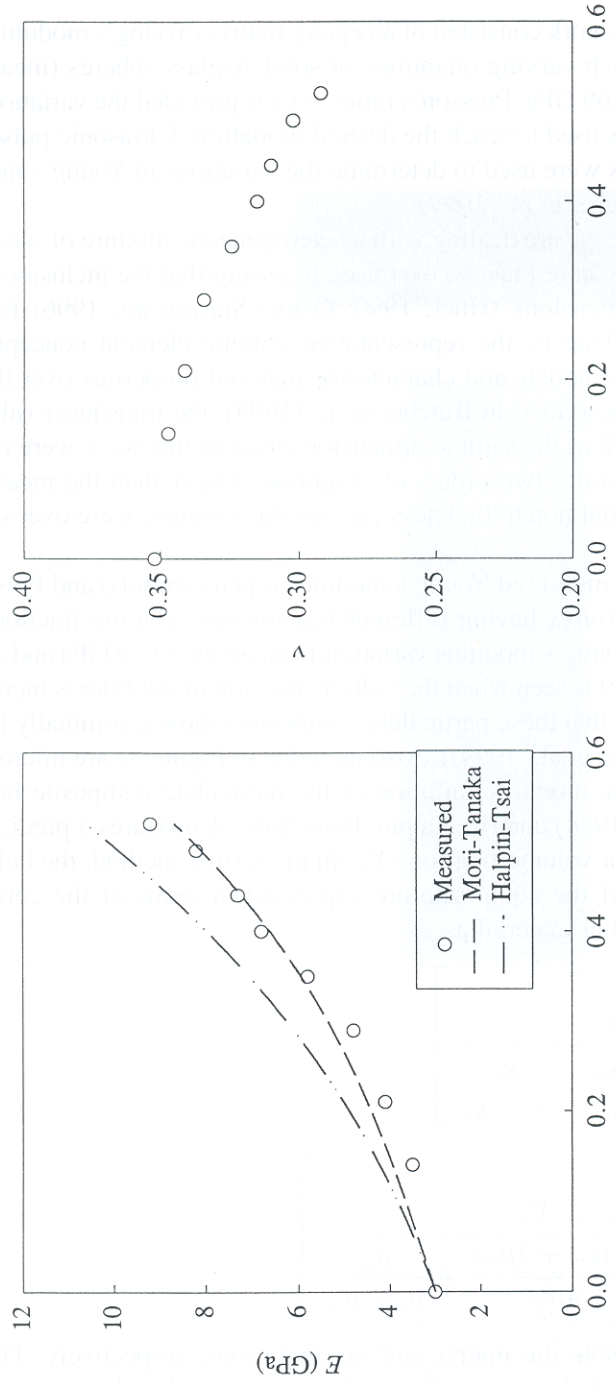

Figure 8. Variation of static (a) Young's modulus and (b) Poisson's ratio with volume fraction of glass spheres in epoxy matrix.

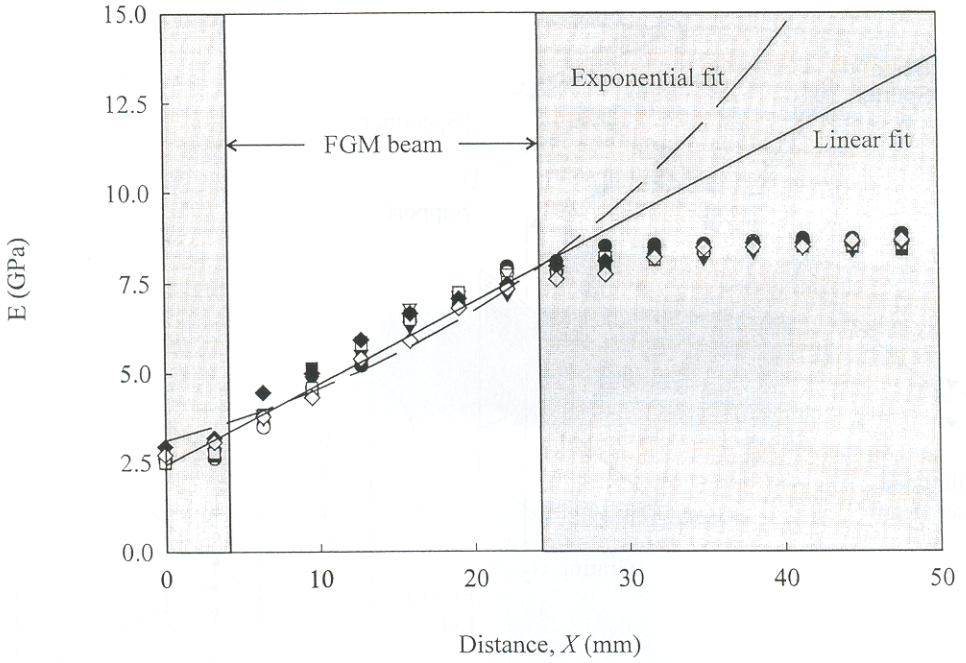

Figure 9. Young's modulus variation in FGM plates (each symbol corresponds to a different casting).

$$E = \frac{E_m(1 + 2s\eta V_f)}{1 - \eta V_f}, \tag{8}$$

where $\eta = [(E_i/E_m) - 1]/[(E_i/E_m) - 2s]$, and s is the aspect ratio of inclusions (in the present case it is 1 for solid spheres). As shown in Figure 8, the Mori–Tanaka estimation follows the experimental measurements rather closely over the entire range of experimental measurements. Although the Halpin–Tsai equation is accurate at very low volume fractions, it consistently over predicts the elastic modulus as the volume fraction increases.

The gravity casting method produced FGMs with a consistent *apparent* elastic modulus gradient between samples, between 3 GPa and 9 GPa. These moduli correspond to pure epoxy and to a composite with a volume fraction of glass spheres in an epoxy matrix of 0.5, respectively. Again, the measurement window used in this characterization was much larger than the scale of heterogeneity and the compositional gradient to enable effective property measurement. Figure 9 shows the modulus variation in several of the plates that were cast. The Poisson's ratio varies smoothly between 0.3 and 0.35 in the graded region (not shown). The first 20 mm of these plates corresponding to the graded region were machined into beam samples of dimensions 120 mm × 20 mm × 6 mm. The beam surfaces were then coated with aluminum to provide the necessary specular surface for optical measurements. Edge notches with root radius of 150 μm and nominal length of 6 mm were cut into the samples using a high speed diamond saw. Subsequent interferometric examination of the samples did not reveal any residual deformations at the crack tip due to sample preparation. It is also important to point out that although the Young's modulus gradient is nearly linear, the results of regression analyses have provided reasonably good exponential fit also ($\alpha = 38.5$ and -38.5 for increasing and decreasing gradients, respectively). These regression fits are shown in Figure 9 and were utilized for extracting the fracture parameters in the experimental and numerical analyses.

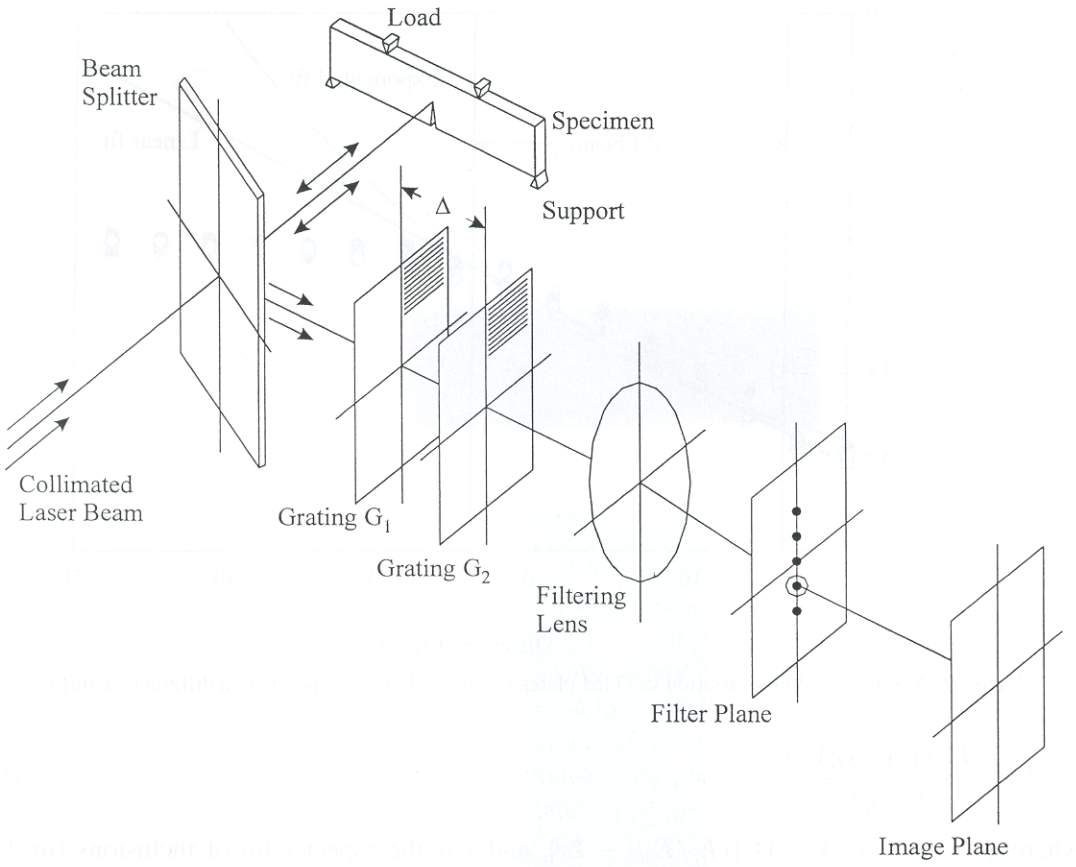

Figure 10. CGS optical set-up used for mapping crack tip deformations in FGMs.

Homogeneous samples having elastic moduli equal to the ones at the crack tips of the FGMs, to within ±2.5%, were also prepared for comparative experimental study. The geometry of these homogeneous samples was identical to that of the FGM samples.

4.2. Coherent gradient sensing

The optical method of *reflection* Coherent Gradient Sensing was used to record crack tip deformations. The working principle for CGS has been reported by Tippur et al., (1991). A schematic of the CGS set-up is shown in Figure 10. An expanded and collimated beam of laser light (approximately 50 mm in diameter) is used to interrogate the specular surface of the specimen. The reflected beam (object wave front) is directed towards a pair of Ronchi gratings using a beam splitter. The object wave front is laterally sheared in the direction perpendicular to grating lines as shown. A filtering lens is used to collect all the sheared wave fronts propagating in discrete directions and the spectral contents appear as a linear array of spots on the back focal plane of the lens. Of these spots, either ±1 diffraction spot is filtered and imaged. The image consists of two laterally sheared light beams with interference fringes in the overlapping area. The information received by the camera represents contours of constant gradients of out-of-plane displacement w with respect to the x- or the y-axis, depending on the orientation of the Ronchi gratings. In the present work, the gratings lines

were oriented perpendicular to the crack. Therefore, the governing equation describes the non-planarity of the sample surface as

$$\frac{\partial w}{\partial x} = \frac{Np}{2\Delta}, \quad N = 0, \pm 1, \pm 2, \ldots , \tag{9}$$

where N denotes fringe orders, p is the pitch of the gratings (25 μm), and Δ is the grating separation distance (47 mm). For plane stress conditions, the out-of-plane displacement w can be related to the in-plane stress components using Hooke's law $\varepsilon_z \cong 2w/B = -v/E(\sigma_x + \sigma y)$, or,

$$w \cong -\frac{vB}{2}\left(\frac{\sigma_x + \sigma_y}{E}\right), \tag{10}$$

where B is the undeformed thickness of the sample.

4.3. Optical measurements

The FGM and homogeneous beam samples were loaded in four-point bending using an Instron-4465 machine in displacement control mode, with a cross-head speed of 0.25 mm per minute. The samples were subjected to symmetric pure bending with constant moment acting over a 60 mm length in the mid-span. The resulting crack tip fringe patterns in FGMs with a crack on the stiff ($E_2/E_1 < 1$) and the compliant sides ($E_2/E_1 > 1$) of the beam are shown in Figures 11a and 11c, respectively. In these cases, the crack tip Young's Moduli were 6.8 GPa and 4.8 GPa, respectively. Further, the far-field applied stress $\sigma_\infty (= 6M/BW^2$, where M is the moment, W and B are the beam height and thickness, respectively) at which the deformations were recorded in these two cases are the same. Homogeneous samples corresponding to the crack tip Young's moduli of these FGMs were also optically investigated. The crack-tip deformation patterns for the homogeneous beams corresponding to the FGMs with the crack on the stiff and compliant side are shown in Figures 11b and 11d, respectively. Note that, the fringe patterns from the homogeneous samples are for the same load level as their FGM counterparts. Finally, as anticipated from Figure 5, one notices far-field behavior of FGMs to be identical to those of homogeneous materials. The sensitivity of the optical measurements is $\sim 0.015°$/fringe.

In each case, the fringes show an overall symmetry about the crack plane indicating a mode-I behavior. However, some differences exist between the fringe patterns in FGMs and between the ones in FGMs and the equivalent homogeneous beams. Figure 12, a plot of the relative position of the fringes along the uncracked ligament of the crack plane, is shown to illustrate these differences. (It is worth noting from the plot that the functional form of these curves is the same, thereby confirming the observations made in the numerical work.) Interestingly, the fringe order, N, values for the FGMs are bounded by their homogeneous counterparts. At a given value of r/B, the value of the fringe order and hence the surface slope for the FGM with the crack on the compliant side indicates smaller deformation than the one for the crack on the stiffer side. Hence, one could expect the crack on the compliant side of the FGM to experience a smaller SIF compared to the one on the stiffer side. Comparison of the fringe data between the FGM with a crack on the compliant side and its homogeneous counterpart suggests a lower surface slope (and lower K_I) for the FGM. On the contrary, the crack tip of the FGM with a crack on the stiffer side suffers steeper surface slope (and hence higher K_I) compared to its homogeneous counterpart.

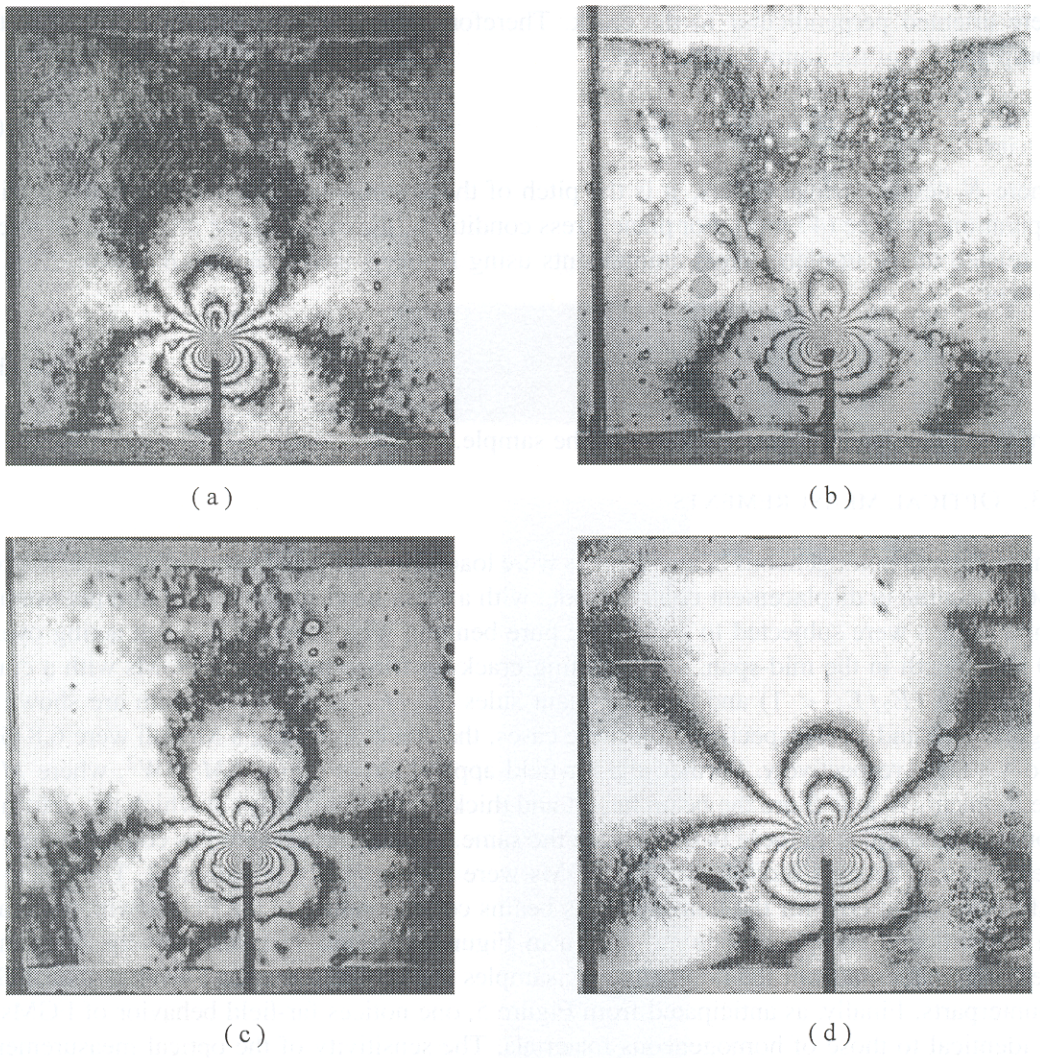

Figure 11. Crack tip interference representing $\delta w/\delta x$ contours for a far-field bending stress $6M/BW^2 = 10.2$ MPa: (a) FGM with $E2/E1 = 0.41$, (b) homogeneous counterpart of (a), (c) FGM with $E2/E1 = 2.23$, (d) homogeneous counterpart of (c), center to center distance from crack to drawn line is approximately 10 mm).

4.4. Quasi-static crack growth

Quasi-static crack growth experiments were conducted on FGMs to evaluate crack growth resistance behavior through direct crack tip measurements. In these, FGM beams with dimensions 120 mm × 37 mm × 6 mm, and crack length a of 7 mm were optically studied. Elastic modulus variations are as shown in Figure 9. Initial edge cracks were cut into different FGM samples, one on the stiffer side, and one on the compliant side. The initial crack tip Young's moduli for these were 7.4 GPa and 4.4 GPa, respectively. The samples were loaded in four-point bending with a constant moment acting over a length of 60 mm in the mid-span. The cross-head speeds were slower in these experiments to accomplish crack tip field imaging with a conventional camera. CGS was used to monitor crack tip deformations. In both

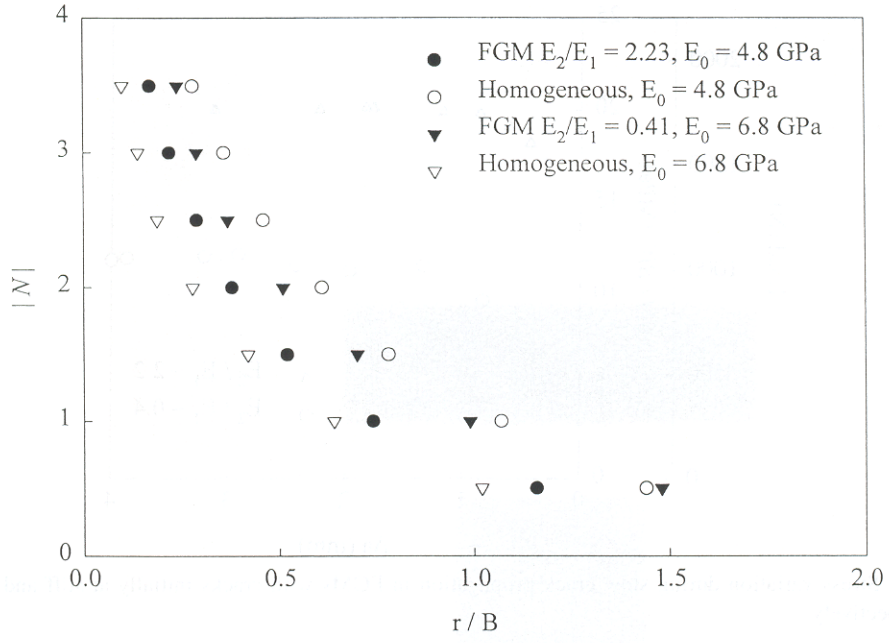

Figure 12. Magnitude of fringe order with location ahead of the crack, for FGMs and their homogeneous counterparts, for far-field bending stress $(6M/BW^2) = 10.2$ MPa.

cases, the crack propagated quasi-statically for a few millimeters before making a transition to unstable dynamic failure. For the beam with a notch on the stiff side, the crack advanced over a length where crack-tip modulus decreased by a factor of 1.08. On the other hand, for the beam with crack on the compliant side, crack advanced over a length where local Young's modulus increase by a factor of 1.12. Figure 13 shows the far-field stresses as a function of crack extension for the two FGM beams. A plateau for the stress levels can be seen in each case. This level is $\sim 50\%$ higher for the crack on the compliant side than for the case where the crack is at the opposite edge of the beam. A CGS interferogram corresponding to 3.5 mm of crack growth for the beam with the crack on the compliant side is shown in Figure 14 as an example. The overall features of the crack tip deformations are similar to the one shown in Figure 11. As the crack propagates, the aluminum thin film coating is damaged along the crack path, resulting in an appearance of a blunt crack tip. However, the deformations further away are unaffected.

5. Extraction of K_I from fringe patterns

Next, the optical interference patterns are used for extracting stress intensity factors in FGM and homogeneous specimens. The basis for the procedures developed here are embedded in the numerical analysis and the experimental observations discussed in Sections 3 and 4. In the present study, a difference interpretation instead of a derivative interpretation of the fringes is adopted for fringe analysis. Accordingly, the fringes are related to the mechanical fields as,

$$\frac{\delta w}{\delta x} \cong -\frac{\delta\left(\frac{vB}{2}\left(\frac{\sigma_x+\sigma_y}{E(x)}\right)\right)}{\delta x} = \frac{Np}{2\Delta}, \tag{11}$$

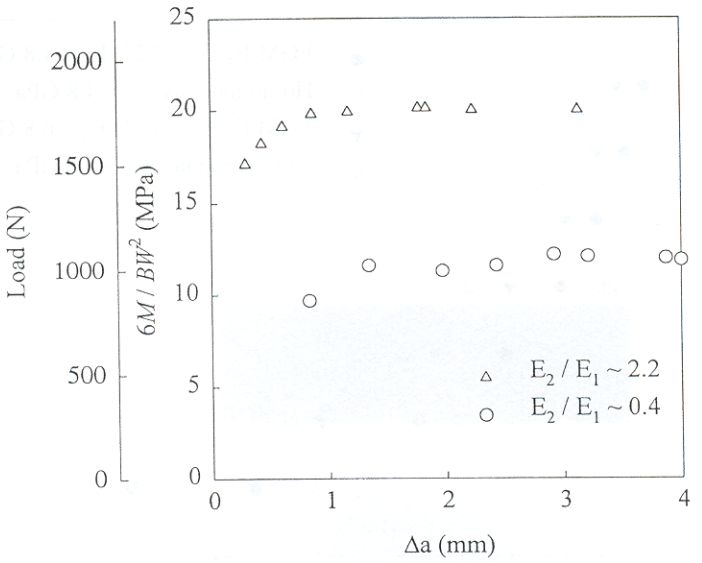

Figure 13. Stress variation during slow crack propagation in FGMs with cracks initially at stiff and compliant edges, respectively.

where $\delta(\bullet)$ is the difference operator and δx is the shearing distance related to the grating pitch p and the grating separation distance Δ (see Figure 10).

5.1. Crack-tip descriptions

It was demonstrated in Section 3 that the functional forms of the near tip field measured from CGS in both radial and hoop directions are the same for both FGM and homogeneous beams. Hence, the method used for analyzing near tip CGS fringes in homogeneous materials will also be used for FGMs. At first, the crack tip field was assumed to be K-dominant. Accordingly for plane stress conditions,

$$w \cong -\frac{vB}{E_0}\left[\frac{K_I}{\sqrt{2\pi r}}\cos\frac{\theta}{2}\right], \tag{12}$$

where E_0 is the crack tip Young's modulus. That would be equivalent to assuming a locally homogeneous material behavior with a Young's modulus E_0 in the crack tip vicinity.

The fringes were digitized around the crack tip and fringe location (r, θ) and fringe order (N) data were extracted. An over-deterministic least-squares analysis was carried out for evaluating the unknown coefficient K_I. The procedure involved was one of minimizing the square of the cumulative error between the measured and the predicted behavior with respect to the unknown coefficient, namely K_I. In this analysis, certain restrictions had to be imposed on the data set to ensure that the measurements come from regions where plane stress conditions likely prevail. It is well known that 3-D effects dominate the crack tip region. For homogeneous materials, a region of dominant 3-D effects exist in the immediate vicinity of the crack tip extending up to $r/B \sim 0.5$ (Rosakis an Ravi-Chandar, 1986). Further, under mode-I loading conditions, triaxial effects are minimal in the range $90° < \theta < 135°$ behind the crack tip (Tippur et al., 1991; Sinha et al., 1997). Although a 3-D crack tip study of deformation fields for FGMs is not available at the moment, in view of the similarities between homogeneous and FGM near tip fields (Figures 3 and 4) discussed earlier, it is reasonable to

Table 1. Comparison of analytical, computed and measured stress intensity factors (MPa$\sqrt{m}$ at a far-field bending stress $6M/BW^2$ of 10.2 MPa

Method of calculation	FGM $E_2/E_1 = 2.23$ $E_0 = 4.8$ GPa	Homogeneous $E_2/E_1 = 1$ $E_0 = 4.8$ GPa	FGM $E_2/E_1 = 0.41$ $E_0 = 6.8$ GPa	Homogeneous $E_2/E_1 = 1$ $E_0 = 6.8$ GPa
FEA (plane stress, $v = 0.32$ or 0.34)	1.27	1.51	1.77[b]	1.46[c]
Analytical (plane strain, v unknown)[a]	1.28	1.52	1.79	1.45
CGS; K-dominant description (plane stress, $v = 0.32$ or 0.34)	1.06	1.26	1.44	1.20
CGS; Williams' expansion field (plane stress, $v = 0.32$ or 0.34)	1.13	1.44	1.80	1.50

[a]Erdogan and Wu (1995).
[b]K_I from plane strain FEA = 2.06 MPa$\sqrt{m}$
[c]K_I from plane strain FEA = 1.69 MPa$\sqrt{m}$

adopt 3-dimensionality observations from homogeneous counterparts while analyzing crack tip fringes in FGMs. Accordingly, data from the region ($r/B > 0.5, 90^\circ < |\theta| < 135^\circ$) was used in the analysis.

When optical data is acquired from regions far away from the crack tip, K-dominance weakens due to the increasing influence of non-singular contributions. In the current study, the measured data generally came from regions beyond $r/B = 0.5$. Hence, inclusion of non-singular terms in the least-squares analysis was warranted. It was demonstrated numerically that in the far-field the functional forms of the measured field quantity are the same for both FGM and homogeneous beams. Furthermore, use of non-singular terms was shown to improve the agreement between the computed field and corresponding asymptotic description. Therefore, two non-singular terms from the Williams' expansion field,

$$w \cong -\frac{vB}{E_0}\left[\frac{K_I}{\sqrt{2\pi r}}\left(\cos\frac{\theta}{2}\right) + c_0 r^0 + c_1 r^{1/2}\cos\frac{\theta}{2} + c_2 r^1 \cos\theta + \cdots\right], \tag{13}$$

were used along with the K-dominant term in the experimental data analysis. The data set used for this was the same one used in the K-dominant analysis and K_I and the higher order coefficients c_1, was evaluated from the least-squares analysis. *Note that CGS being a measure of the derivative of w, the constant c_0 (or the so-called T-stress) does not contribute to the CGS fringes.*

5.2. Results and discussion

Both FGM specimens were subjected to a far-field bending stress $6M/BW^2$ of 10.2 MPa. The FGM sample with a crack located on its compliant side had a crack tip modulus $E_0 = 4.8$ GPa, and a modulus ratio (E_2/E_1) between its two edges of 2.23. The other FGM sample, with an edge crack on the stiff side had a crack tip modulus $E_0 = 6.8$ GPa, and a modulus ratio of 0.41. The homogeneous samples with moduli corresponding to those at the crack tips (E_0) of

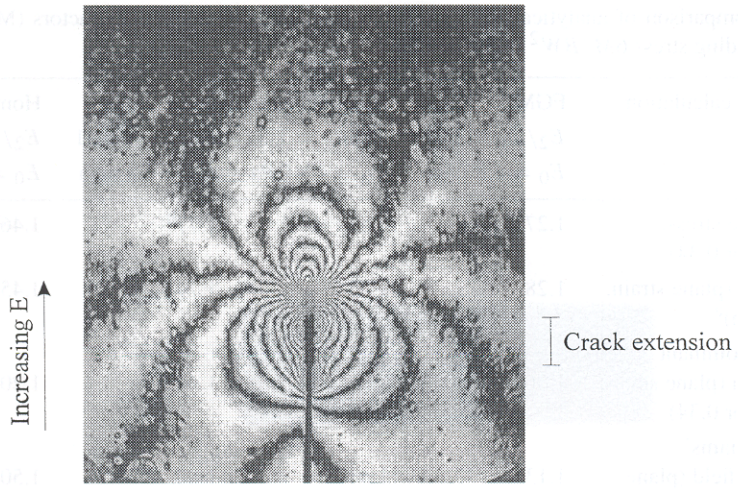

Figure 14. Reflection CGS fringes representing $\delta w/\delta x$ near a quasi-statically growing crack in an FGM with a crack on the compliant side.

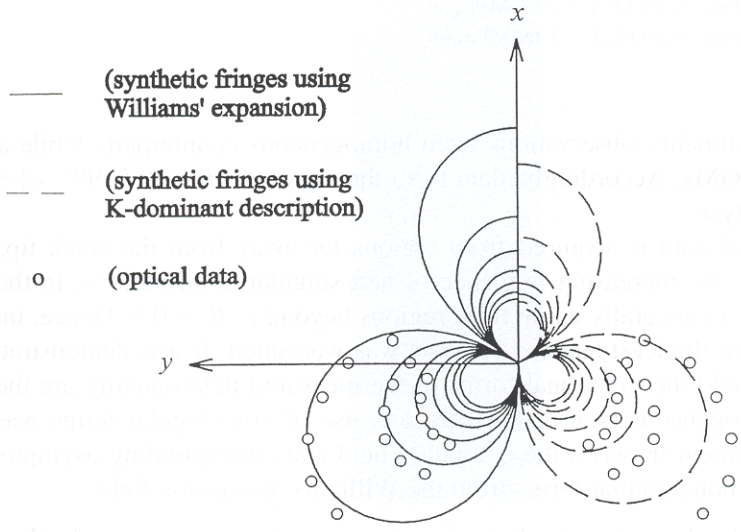

Figure 15. Optical data analysis for the FGM with a crack on the glass-rich side using least-squares method.

the FGMs were subjected to far-field stresses identical to those of their FGM counterparts, so that a direct comparison could be made.

A comparison of the mode-I stress intensity factors obtained by the two methods of analysis of interferograms is presented in Table 1. Under the premise of K-dominance, the experimental values of K_I for the FGMs are about 20% lower than those predicted by the numerical calculations and analytical results. (Note that the analytical results for FGMs are for a value of Poisson's ratio that is not reported, whereas finite element simulations and experiments assume plane stress conditions, with Poisson's ratios of 0.34 and 0.32 for the beams with cracks on the stiff and compliant sides, respectively.) When least-squares analysis based on Williams' expansion field was used, the values of stress intensity factors improved and the error between the numerical and experimental results reduced to 10% or less. (Also shown in the table for completeness are the values of SIF determined using plane strain FEA simulations

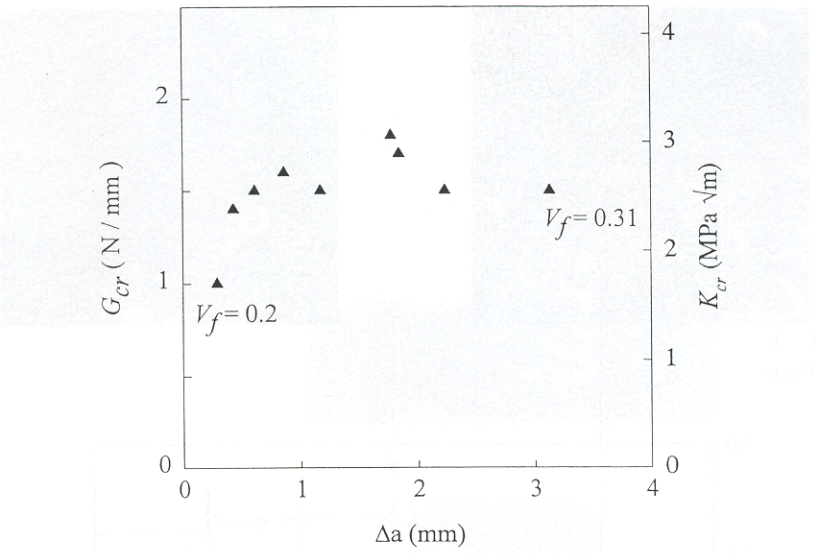

Figure 16. Crack growth resistance for FGM with crack on the compliant side.

for the case of FGM with $E_2/E_1 = 0.41$ and its homogeneous counterpart. The computed values of SIF are higher than the plane stress counterparts by about 15% and therefore deviate from the optical evaluations more substantially.) An example of the agreement between the experimental data and synthetic fringes generated by the least-squares analysis for the FGM with a crack on the stiff side is shown in Figure 15. The open circles represent optical data from both dark and light fringes (Figure 11a). The broken lines represent synthetic fringes based on K-dominant assumptions, whereas the solid lines are those based on Williams' expansion field description. Evidently, the match between data and the synthetic fringes improves with the additional of non-singular terms to the field description.

The stress intensity factors for FGM and homogeneous samples are compared next. An FGM with a crack on the stiff side of the beam experiences higher stress intensification by a factor of approximately 1.2 when compared to its homogeneous counterpart subjected to an identical far-field loading. On the contrary, an FGM with a crack on the compliant side of the beam experiences lower stress intensification by a factor of 0.8 when compared to its homogeneous counterpart. Thus, the crack on the stiff side of the FGM experiences higher stress intensification by a factor of 1.5 when compared to the one with the crack on the compliant side. This ratio between the two values is similar to the ratio between far-field stresses during steady state crack growth as in Figure 13.

Since Williams' expansion has proven useful in refining fringe analyses in FGMs, it was also used for extracting stress intensity factors for growing cracks. Figure 16 shows the variation in measured crack driving force and stress intensity factor for the case with the crack on the compliant side of the FGM, as it propagates over the range of stable crack growth. The initial increase in stress intensification is immediately followed by a plateau. The onset of crack growth in a material with a preexisting crack occurring only at values of fracture toughness, it can be surmised that the symbols plotted on Figure 16 represent local resistance to crack growth of the FGM material. Interestingly, the measured crack growth resistance attains a nearly constant value (0.5 mm $< \Delta a <$ 3 mm) after an initial increase in the early stages of crack growth ($<$ 0.5 mm). This is somewhat unexpected since the material shows a

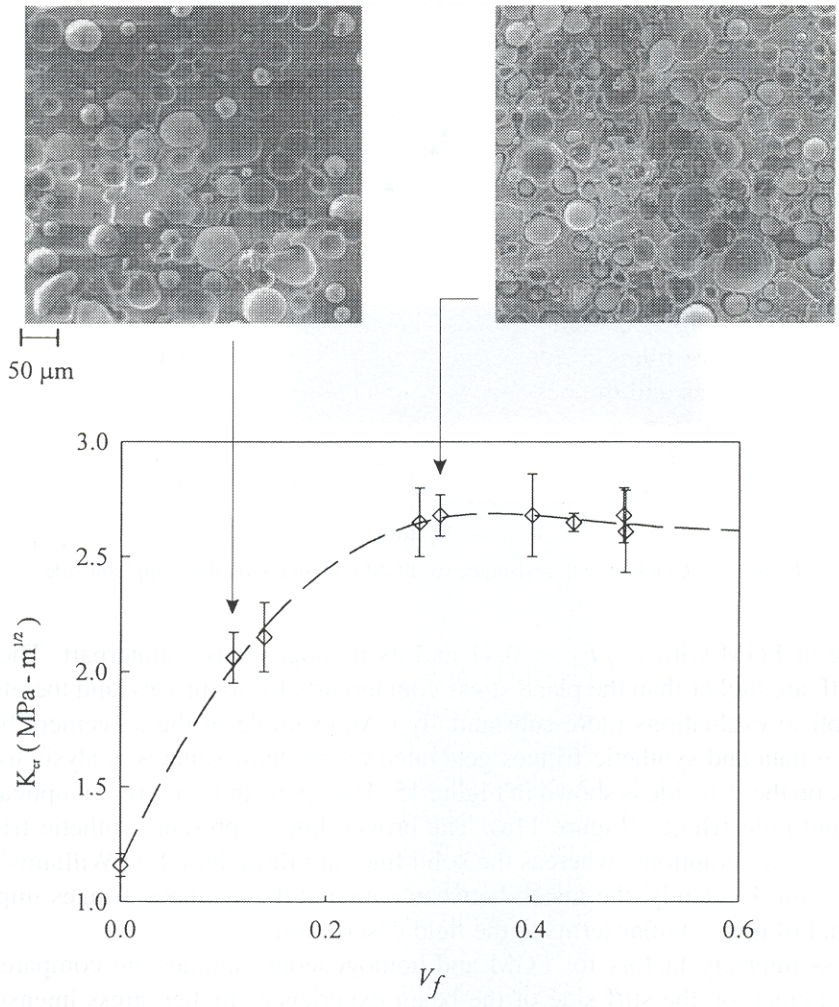

Figure 17. Variation of fracture toughness with volume fraction of glass spheres in the epoxy matrix.

monotonically increasing Young's modulus in this case. To ascertain the above, the fracture toughness of the material for various volume fractions of the filler material was determined. Beam samples with edge notches were separately prepared. Sharp cracks were introduced into these samples by controlled driving of a wedge between the flanks of pre-cut notches to 'pop' the notch tip by a few millimeters. Fracture tests were conducted on these homogeneous cracked beams, each having a different but constant volume fraction. All samples showed a linear increase in load with displacement, and a sudden drop at the breaking point. The critical values of K_I from measured breaking loads are plotted in Figure 17 as a function of volume fraction of the filler material, V_f The apparent fracture toughness of the material increased monotonically until about $V_f = 0.25$. These increases are similar to the observations of Maloney et al., (1987) for small volume fraction of glass fillers. Beyond this value of V_f, the K_{Icr} value essentially remains constant at ~ 2.75 MPa $\sqrt{m}$, in the range $V_f = 0.25$–0.50. This is also the value at which the stress intensity factor levels during the quasi-static crack growth investigation, thus confirming the optical measurements.

The increase in the apparent fracture toughness over $0 < V_f < 0.25$ could be attributed to the fact that filler particles hinder crack propagation, compelling the crack to follow filler-matrix interfaces and/or to branch and circumvent the particles (see insets in Figure 17). The SEM micrographs of the fractured surfaces indicate that the former of the two mechanisms appears to be the dominant mode of failure (interfacial separation between particles and matrix can be seen with either particle footprint in the matrix or the particle residing in a epoxy cavity). Thus, the surface area created by crack growth is enhanced by a factor of two and if interfacial fracture toughness is better than half that of the matrix, apparent fracture toughness of the composite will be higher. A similar observation is advanced by Parameswaran and Shukla (2000) regarding monotonic increase in fracture toughness with small filler volume fractions of *cenosphere* fillers in polyester. As the volume fraction increases (inset at volume fraction 0.3), pores and the possibility of unwetted neighboring glass spheres acting as microdefects increases (Figure 17). In these situations, the overall fracture toughness will be essentially a competition between the enhancement due to crack filler-matrix interfacial failure and branching and reduction from coalescence of microdefects, thereby leaving the measured fracture toughness to be nearly constant.

6. Conclusions

The behavior of the crack tip stress field for FGM beams subjected to pure bending, with an edge crack parallel to the elastic modulus gradient has been examined. The FGM samples were fabricated using gravity casting of a particulate composite of solid A-glass spheres in an epoxy matrix. Elastic properties of this particulate composite and fracture toughness for different volume fractions of the filler material are reported. Microscale heterogeneity in the material is homogenized by the macroscale measurements to obtain *apparent* Young's modulus variation of the composite that is well described by Mori-Tanaka estimates for a two-phase mixture. A three-fold increase in Young's modulus (3 to 9 GPa) is recorded when the volume fraction of the filler is varied from zero to 50%. Crack tip fields have been interferometrically measured in FGM and homogeneous samples using coherent gradient sensing and deformation patterns have been compared. Complementary numerical simulations were undertaken for examining the crack tip behavior and deformation characteristics. The results suggest that the functional form of near tip and far-field deformations measured using CGS are similar in FGM and homogeneous beams. Based on these results, crack tip stress measurements from optical interference patterns have been performed using descriptions based on K-dominance as well as a field affected by non-singular contributions. The measurements based on K-dominant descriptions in FGMs are within 20% of the plane stress computed/analytical results. The inclusion of non-singular effects in the experimental analysis seems to improve the measurements to within 10% of the anticipated results under plane stress assumption. Further, the elastic gradient causes the FGM beam with a crack on the glass-rich (stiff) side experience higher value of K_I when compared to its homogeneous counterpart when subjected to identical far-field loading. On the other hand, the FGM beam with a crack on the epoxy-rich (compliant) side of the beam experiences a lower K_I compared to its homogeneous counterpart. The measurements thus suggest that elastic gradients reduce crack tip stress intensification in an FGM with a crack on the compliant side ($E2/E1 \sim 2.2$) by a factor of about 1.5 when compared to the one with the crack on the stiff side ($E2/E1 \sim 0.4$). Crack tip deformations near quasi-statically growing cracks in FGMs are optically mapped and the growth characteristics during

stable growth are determined. The measurements suggest a nearly constant fracture toughness in the region where the filler volume fraction is > 0.25. The observations are supported by independent crack initiation toughness tests conducted using homogeneous compositions of different but constant volume fractions.

Acknowledgements

The support of this research by ARO Solid Mechanics Program (DAAG55-97-1-0110) and NSF Materials Program (CMS-9622055) is gratefully acknowledged.

References

Bao, G. and Cai, H. (1997). Delamination cracking in functionally graded coating/metal substrate systems. *Acta Materialia* **45**, 1055–1066.

Butcher, R.J., Rousseau, C.-E. and Tippur, H.V. (1999). A functionally graded particulate composite: preparation, measurements and failure analysis. *Acta Materialia* **47**, 259–268.

Delale, F. and Erdogan, F. (1983). The crack problem for a nonhomogeneous plane. *ASME Journal of Applied Mechanics* **50**, 609–614.

Eischen, J.W. (1987). Fracture of nonhomogeneous materials. *International Journal of Fracture* **34**, 3–22.

Erdogan, F. (1995). Fracture mechanics of functionally graded materials. *Composites Engineering* **5**, 753–770.

Giannakopoulos, A.E. and Suresh, S. (1997). Indentation of solids with gradients in elastic properties: Part I. Point force. *International Journal of Solids Structures* **34**, 2357–2392.

Honein, T. and Herrmann, G. (1997). Conservation laws in nonhomogeneous plane elastostatics. *Journal of the Mechanics and Physics of Solids* **45**, 789–805.

Huet, C. (19). Application of variational concepts to size effects in elastic heterogeneous bodies. *Journal of the Mechanics and Physics of Solids* **38**, 813–841.

Jin, Z.-H. and Batra, R.C. (1996). Some basic fracture mechanics concepts in functionally graded materials. *Journal of the Mechanics and Physics of Solids* **44**, 1221–1235.

Jin, Z.-H. and Noda, N. (1994). Crack-tip singular fields in nonhomogeneous materials. *ASME Journal of Applied Mechanics* **61**, 738–740.

Krishnaswamy, S., Rosakis, A.J. and Rarichandran, G. (1991). On the extent of dominance of asymptotic ,elastodynamic crack-tip fields: Part II. Numerical investigation of three-dimensional and transient effects. *ASME Journal of Applied Mechanics* **58**, 95–103.

Lee, Y.-D. and Erdogan, F. (1995). Residual/thermal stresses in FGM and laminated thermal barrier coatings. *International Journal of Fracture* **69**, 145–165.

Marur, P.R. and Tippur, H.V. (1998). Evaluation of mechanical properties of functionally graded materials. *Journal of Testing and Evaluation* **26**, 539–545.

Marur, P.R. and Tippur, H.V. (2000). Dynamic response of bimaterial and graded interface cracks under impact loading. *International Journal of Fracture* **103**, 103–109.

Moloney, A.C., Kausch, H.H., Kaiser, T. and Beer, H.R. (1987). Parameters determining the strength and toughness of particulate filled epoxide resins. *Journal of Materials Science* **22**, 381–393.

Ostoja-Starzewski, M., Jasiuk, I., Wang, W. and Alzebdeh, K. Composites with functionalled graded interphases: Mesocontinuum concept and effective tansverse conductivity. *Acta Materialia* **44**, 2057–2066. 2057 066.

Parameswaran, V. and Shukla, A. (2000). Processing and characterization of a model functionally gradient material. *Journal of Materials Science* **35**, 21–29.

Rice, J.R. (1968). A path of independent integral and the approximate analysis of strain concentration by notches and cracks. *ASME Journal of Applied Mechanics* **35**, 379–386.

Rosakis, A.J. and Ravi-Chandar, K. (1986). On crack-tip stress state: An experimental evaluation of three-dimensional effects. *International Journal of Solids and Structures* **22**, 121–138.

Rousseau, C.-E. (2000). Evaluation of crack tip fields and fracture parameters in functionally graded materials. Ph.D. Dissertation, Auburn University.

Rousseau, C.-E. and Tippur, H.V. (2000). Compositionally graded materials with cracks normal to the elastic gradient. *Acta Materialia* **48**, 4021–4033.

Rousseau, C.-E. and Tippur, H.V. (2001). Dynamic fracture of compositionally graded materials with cracks along the elastic gradient: Experiments and analysis. *Mechanics of Materials* **33**, pp. 403–421.

Sinha, J.K., Tippur, H.V. and Xu, L. (1997). An interferometric and finite element investigation of interfacial crack tip fields: Role of mode-mixity on 3-D stress variations. *International Journal of Solids and Structures* **34**, 741-754.

Tippur, H.V., Krishnaswamy, S. and Rosakis, A.J. (1991). A coherent gradient sensor for crack tip deformation measurements: Analysis and experimental results. *International Journal of Fracture* **48**, 193-204.

Weng, G.J. (1984). Some elastic properties of reinforced solids, with special reference to isotropic ones containing spherical inclusions. *International Journal of Engineering Sciences* **22**, 845–856.

Whitney, J.M., Daniel, I.M. and Pipes, R.B. (1984). *Experimental Mechanics of Fiber Reinforced Composite Materials*, SEM Monograph No. 4, Prentice Hall, Inc., NJ.

Williams, M.L. (1957). On the stress distribution at the base of a stationary crack. *ASME Journal of Applied Mechanics* **24**, 109–114.